Energy 102 (2016) 54–64

Contents lists available at ScienceDirect

Energy

journal homepage: www.elsevier.com/locate/energy

Gas/particle two-phase flow characteristics of a down-fired 350 MWe supercritical utility boiler at different tertiary air ratios

Chunlong Liu [a, b], Zhengqi Li [b, *], Lingyan Zeng [b], Qinghua Zhang [c], Richa Hu [a], Xusheng Zhang [a], Liang Guo [a], Yong Huang [a], Xianwei Yang [a], Liheng Chen [a]

[a] Changchun Institute of Optics, Fine Mechanics and Physics, Chinese Academy of Sciences, Changchun 130033, China
[b] School of Energy Science and Engineering, Harbin Institute of Technology, 92 West Dazhi Street, Harbin 150001, China
[c] Mechanical and Electronic Engineering Department, Heilongjiang College of Coal Career Technical, 1 Gongli Street, Shuangyashan 155100, China

ARTICLE INFO

Article history:
Received 13 May 2015
Received in revised form
6 January 2016
Accepted 4 February 2016
Available online 4 March 2016

Keywords:
Down-fired boiler
Gas–solid two-phase
Secondary-air ratios
Phase-doppler anemometry

ABSTRACT

To investigate the influence of the air distribution in the down-fired boiler which adopts the multi-injection and multi-stage combustion technology, a 1:20 small-scale model of a down-fired pulverized-coal 35 MWe supercritical utility boiler was set up to study the gas–solid two-phase flow characteristics at different tertiary air ratios by using PDA (particle dynamics anemometer) measurement. Gas and particles move downward near the front/rear wall and toward the furnace center area. A U shape flow field formed in the half furnace, the volume flow flux of the particles exhibited a peak beneath the primary air nozzles, the value of the peak decreased as the air flow injected downward In the area of the tertiary air nozzles, the horizontal/vertical fluctuation velocity for gas/solid phases near the furnace hopper wall increased rapidly, the airflow mixed here intensely. As the tertiary air ratio increases, the maximum volume flux increased obviously, and was conducive for the pulverized coal to ignite. Maximum gas-phase vertical velocity and maximum solid-phase particles volume flux moved further away from the hopper. This feature reduced the possibility of the occurrence of both flushing and slagging of the hopper.

1. Introduction

About 30% of the power station coal in China comprises anthracite and lean coal [1]. Fuel is difficult to ignite because of their low volatile content, and requires a longer time to burnout and result in a high coke content [2,3]. To strengthen the combustion, before the 1990s, the Chinese power plant boilers mainly adopted direct-flow burners with tangential firing mode, with a few using the swirl burner wall-firing mode. For others, a variety of burners were tried, such as swirl precombustion chambers and flame stabilization equipment direct-flow coal burners [4,5]. The W-shaped combustion technology is widely used throughout the world as a means of achieving the efficient burning of anthracite and lean coal, owing to the characteristics of a long journey for the flame and a uniform heat load distribution along the width of the furnace. China introduced this technology from abroad in the late 1980s, and the capacity has now reached 41,000 MW.

However in practical operation, the down-fired boilers have significant problems, such as high fly ash carbon content (typically in the range 8–15%), and high NO*x* emissions (generally over 1300 mg/m^3, at 6% O_2) [6–10]. Refs. [6,7] investigated the 660 MW Foster Wheeler (FW) down-fired boiler, which was the largest capacity boiler in the world. Because large quantity of secondary air was supplied from F layer, high NO*x* emission was formed in this region. Ref. [8] investigated the 300 MW Babcock & Wilcox (B&W) down-fired boiler, which used unique swirl burner. Secondary air was supplied from the burner, which cause the primary air and secondary air mixed earlier. Ref. [9] investigated combustion characteristics and NO*x* emissions of the split burner which manufactured by Babcock & Wilcox (B&W). The pulverized coal was surrounded by secondary air which formed large quantity of NO*x*. In addition, some boilers suffer from asymmetric combustion in the furnace [9,11–13]. Several studies have been undertaken to analyze the causes of these problems. Fang et al. investigated the slagging characteristics by numerical

* Corresponding author. Tel.: +86 4518648854; fax: +86 45186412528.
E-mail address: green@hit.edu.cn (Z. Li).

http://dx.doi.org/10.1016/j.energy.2016.02.016
0360-5442/

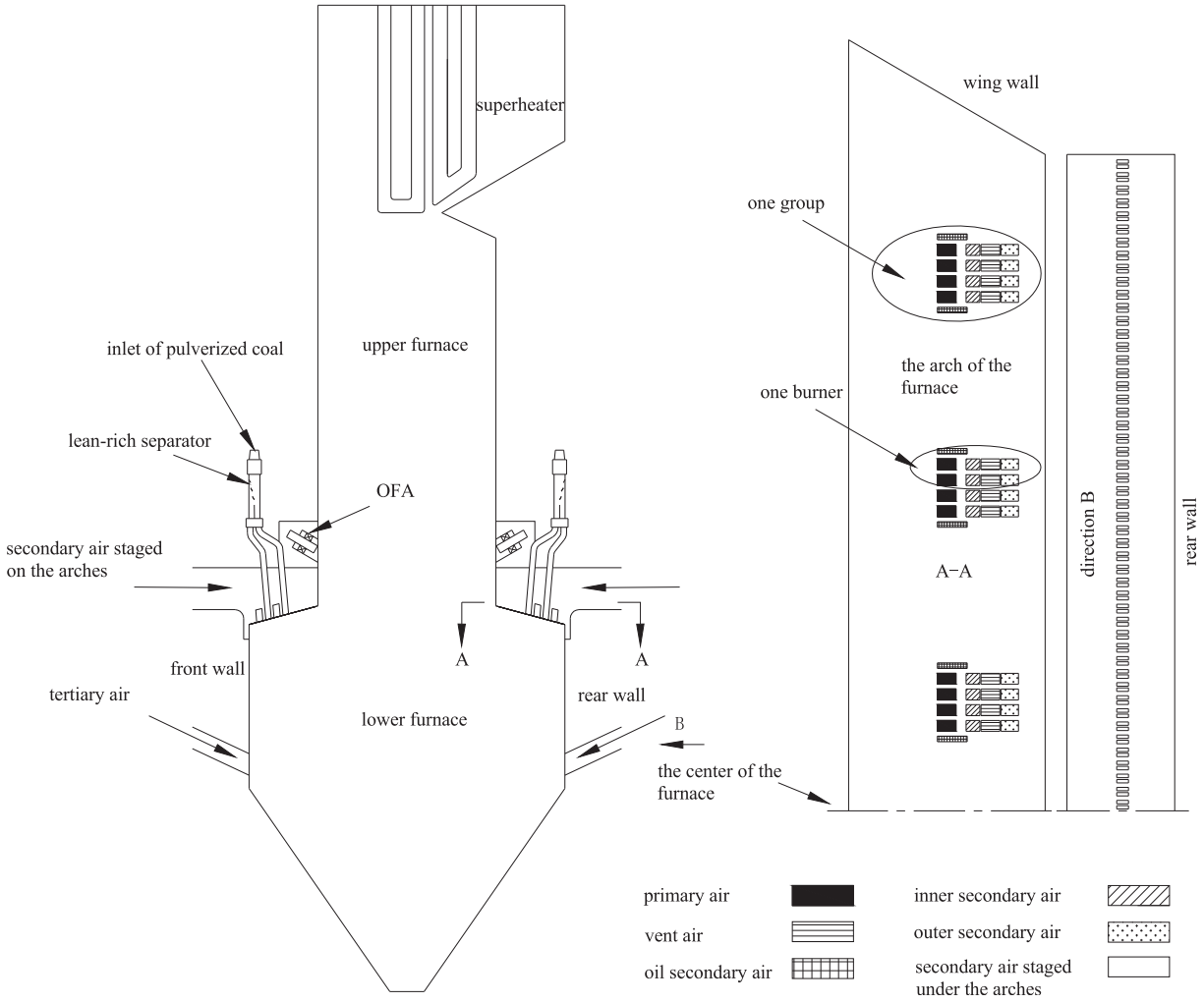

Fig. 1. Combustion system of the down-fired boiler.

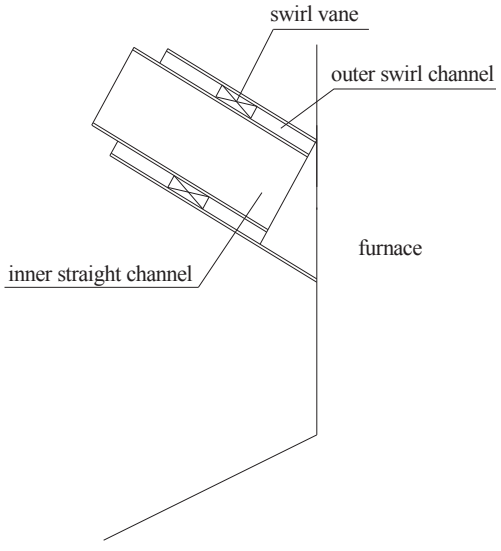

Fig. 2. Structure of OFA air nozzle.

simulation of a 300 MWe Foster Wheeler (FW) down-fired boiler and concluded that the wing and side walls of the lower furnace are the main slagging areas [14]. Fan et al. used numerical simulation methods to investigate the flow, combustion, and NO*x* emissions within a 300 MWe down-fired boiler manufactured by Babcock & Wilcox (B&W) [15]. Cañadas et al. and Fueyo et al. studied the parametric tuning of operating conditions for NO*x* reduction in FW down-fired boilers [16,17], whereas Leisse and Lasthaus and Garcia-Mallolet et al. researched OFA (over-fire air) applications [18,19]. Zhou et al. have shown that in a down-fired boiler the swirl intensity of secondary air notably affected the aerodynamic characteristics [20].

The essence of the pulverized coal flow in the furnace is gas–solid two-phase flow when the boiler is in operation. Studies should therefore be directed at the gas–solid two-phase flow characteristics to obtain the rules governing the movement of the pulverized coal in the furnace. For gas–solid two-phase flow characteristics, researchers have usually adopted experimental studies. For example, Fan et al. studied the characteristics of gas flow in the burnout area and gas/particle flows under the front panel superheater of a 300 MWe tangential firing boiler [21]. In studies of the flow characteristics in the furnace of down-fired boilers, a widely used method involves the use of a PDA (particle dynamics anemometer) system. Ren studied features such as flow; combustion and NO*x* formation characteristics for a 300 MW

Table 1
Characteristics of design coal ultimate analysis and proximate analysis.

Name	Symbol	Unit	Design coal
Carbon	C_{ar}	%	55.95
Hydrogen	Y_{ar}	%	2.34
Hydrogen	O_{ar}	%	1.12
Nitrogen	N_{ar}	%	0.83
Sulfur	S_{ar}	%	4.53
Ash	A_{ar}	%	30.05
Moisture	M_{ar}	%	5.18
Dry ash-free basis volatile matter	V_{daf}	%	9.50
Received low calorific value	$Q_{net,ar}$	kJ/kg	21327

down-fired boiler produced by Foster Wheeler (FW), and suggested that a high efficiency and low NO*x* production could be achieved for the down-fired boiler [22,23]. Kuang has carried out several experimental studies on a 600 MW down-fired boiler produced by Babcock & Wilcox (B&W), and proposed some options for retrofitting [24–26].

Based on several investigations of current down-fired boilers, Li et al. proposed the use of multi-injection and multi-stage combustion technology and using this technology to design a 350 MWe supercritical utility boiler [27]. The total air of the down-fired boiler is divided into five parts: The over-fired nozzles arranged on the upper furnace, the primary air (include air and 85% pulverized coal into the furnace), vent air (include air and 15% pulverized coal into the furnace), secondary air (inner and outer secondary air on the arches) arranged on the arches and the tertiary air arranged in the lower furnace. According to cold-airflow experiments at different over-fire air ratios using a small-scale furnace, use of an over-fire air ratio greater than 19.1% was recommended. So this over-fired ratio was adopted in this paper [27].

The gas–solid two-phase flow field in the actual operation in the boiler was mainly affected by the air distribution of the over-arch air and under-arch air, thus to adjust the combustion condition and relieve the water-wall slagging [26]. So it is necessary to study the boiler air distribution affect on the gas–solid two-phase flow characteristic. A gas–solid two-phase model was built using a scale of 1:20 for a 350 MWe supercritical utility boiler, using a PDA system for measurement. According to experience of Ref. [28], when the staged-air ratios were larger than 25%, the flow field could be asymmetric. The OFA ratio, primary air ratio and vent air ratio were maintained constant during the experiments, with various values of the tertiary air ratio (15%, 20% and 24.16%) to study the effect of the tertiary air ratio on the gas–solid two-phase flow characteristics in the furnace. Excess air supply ratio at furnace outlet were same, the sum of secondary air ratio and tertiary air ratio flow was 54.66%. When varying the territory air ratios, the secondary air ratios were also changed. The experimental results provide a reference for practical operation, renovation of the boiler, and can also offer a basis for the design of a similarly configured down-fired boiler.

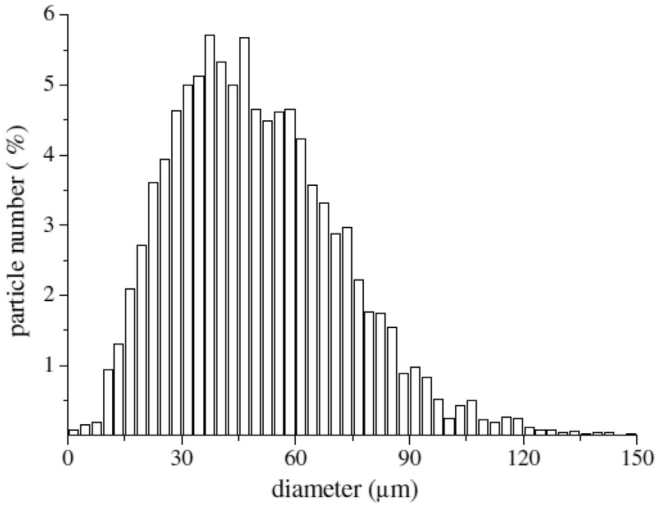

Fig. 3. Particle size distribution.

2. Experiment set up

Combustion system of the down-fired boiler is shown in Fig. 1. The boiler has 24 burners, arranged on the arches. The two adjacent burners are arranged centrally. The secondary air is divided into three parts, namely the inner and outer secondary air on the arches, the tertiary air and the OFA arranged in the upper furnace. In each burner, four successive nozzles are arranged from the furnace center to the front/rear wall; these convey the primary air, the inner secondary air, the vent air and the outer secondary air. These nozzles incline to the furnace center and 5° angle to the vertical direction. Tertiary air is injected into the furnace at a 25° declination angle. Both the front and rear walls have 13 OFA nozzles which are symmetrically arranged in the upper furnace. Each nozzle adopts the structure of inner straight air and outer swirl air. Structure of OFA air nozzle is shown in Fig. 2. There are 16 axial bending swirl vanes in the outer nozzle and no vane in the inner nozzle. The design coal and the checked coal are all anthracite, design pulverized-coal fineness R_{90} is 6%. The ultimate analysis and proximate analysis are listed in Table 1.The boiler uses multi-injection and multi-stage combustion technology, the essence of which is to inject the primary air near the furnace center to a larger downward depth by means of high-speed secondary air. This air is reinjected by the tertiary air, thereby making full use of the lower furnace space. The pulverized coal is easy to ignite, owing to the low velocity flow of primary air near the furnace center. The pulverized coal experiences a long contact time arising from the injection of secondary air that ensures efficient combustion. Finally, tertiary air and OFA lead to a reduction in the formation of NOx. More considerations of multi-injection and multi-stage combustion technology are available [29].

The similarity criteria for particle laden flows are quite complex and difficult to satisfy. Usually, some of the criteria of less importance were ignored. The main criteria in this paper are as follows:

1. Geometric similarity: the ratio of model rig to full scale boiler is 1:20 and is therefore convenient for measurement using the PDA system.
2. Under the same conditions for the model and prototype, the ratio of momentum flux rate of model air flows should be consistent with the full-scale boiler.
3. Under the same conditions for the model and prototype, the Reynolds number of the primary and secondary air exits must be larger than 10,000 to ensure the air flows are self-modeling.
4. In gas/particle experiments, the coarse glass bead diameter is 48.15 μm while that of the fine glass beads is 14.35 μm. Particle size distribution is shown in Fig. 3. The gas/particle flow in the furnace is forced flow and particle size is no more than 200 μm. So the Froude criterion was ignored in the present gas/particle flow experiments.

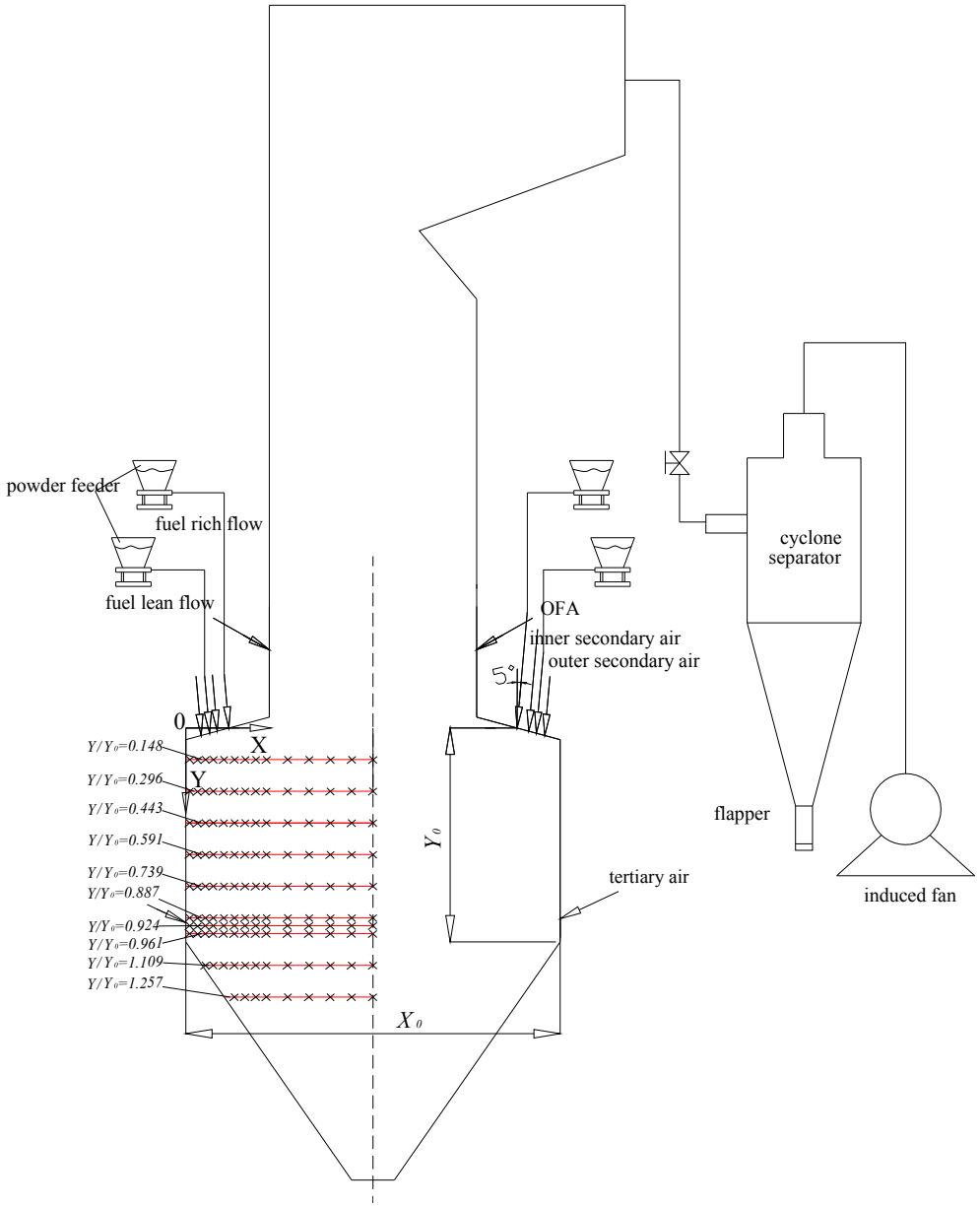

Fig. 4. Schematic diagram of the measurement points and the data processing sections.

When the mentioned criteria were satisfied, the gas/particle two-phase flow was similar to the flow conditions in the real furnace.

The three-dimensional PDA (particle dynamics anemometer), which has gained much use, can provide a wide range of flow field information [21,30–32]. The PDA principle is presented in detail elsewhere [22,23]. The schematic diagram of the measurement points and data processing sections are presented in Fig. 4. The scaled model includes modeling part of the furnace, primary and vent air pipe, secondary air bellows on the arch, a tertiary air bellow, an over-fire bellow, inlet air control pipeline, a pulverized coal feeder, a cyclone separator, an air locker, an induced-draft fan and a PDA system. The intersection of the central height of the primary air nozzle exit and the front wall is defined as the coordinate origin, X_0 stands for the horizontal distance in the lower furnace between the front and rear walls, X represents the distance from the coordinate origin to the measurement point in the horizontal direction, Y_0 is the vertical distance, which is from the upper edge of the furnace hopper to the outlet of the fuel-rich flow nozzle, and Y denotes the vertical distance between the measurement point and the outlet of the fuel-rich flow nozzle. Vy is the vertical velocity of gas or particles at the measurement point, and Vy_0 is the vertical velocity of the primary air outlet. The primary and secondary air flux was measured using Venturi tube flow meters. The airflow rate measurement error is less than 10%.

Photos of the experiment set up are shown in Fig. 5. Fuel rich flow, fuel lean flow, OFA nozzle, tertiary air box, measurement zone, PDA instrument and measurement point are presented.

The source of signals of PDA is the scattering light from the particles in the fluid flow. Geometric and physical parameters of the particles influence the quality of signals obtained from the photo detector of the PDA system. If particles are small enough to be in dynamic equilibrium with the fluid flow then the particle velocity

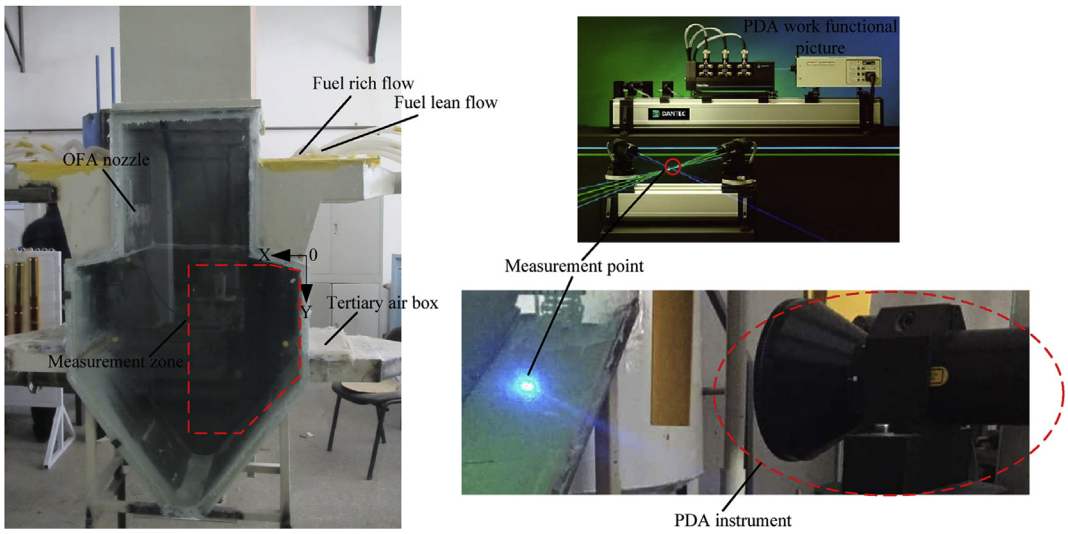

Fig. 5. Photos of the experiment set up.

Table 2
PDA parameters for the measurable range and measurement error.

Quantity	Velocity	Particle diameter	Particle concentration
Measurable range	0-500 m/s	0.5–1000 μm	0–10^6 particles/cm^3
Measurement error	1%	4%	15%

Table 3
Exit parameters of each airflow at different tertiary air ratios.

Tertiary air ratio (%)	15	20	24.16
Primary air velocity (m/s)	10	10	10
Primary air ratio (%)	7.26	7.26	7.26
Primary air particle concentration (particle/air, kg/kg)	0.94	0.94	0.94
Vent air velocity (m/s)	10	10	10
Vent air ratio (%)	10.9	10.9	10.9
Vent air particle concentration (particle/air, kg/kg)	0.17	0.17	0.17
Secondary air velocity (m/s)	25.84	22.87	20.37
Secondary air ratio (%)	39.66	34.66	30.5
Tertiary air velocity (m/s)	12.60	16.86	20.37
OFA air velocity (m/s)	12.16	12.16	12.16
OFA air ratio (%)	19.1	19.1	19.1

can be safely assumed to be equal to the fluid velocity. For fine particles with diameters from 0 to 10 μm, the particle Reynolds number is less than 1; thus these particle flows are in the Stokes regime where particles can trace the gas motions tightly. Consequently, particles with diameters from 0 to 10 μm were used to trace the airflow in the present experiments, and particles with diameters from 10 to 100 μm were used to signify particle phase flow. Particles with diameters between 0 and 100 μm were used for analysis of the particle-volume flux. The relaxation time of the particles was defined to describe the mixing velocity of the gas and solid phases. For the two diameters mentioned above, the relaxation times are less than 1.5×10^{-2} s, therefore the gas–solid two-phase flow condition in the present lab-scale experiment is able to reflect the operating boiler flow condition preferably [22]. The measurable range of PDA parameters and measurement errors are listed in Table 2. To obtain the gas–solid two-phase flow characteristics three conditions were examined, with the tertiary air ratio set at 15%, 20% and 24.16%. The operating conditions are shown in Table 3.

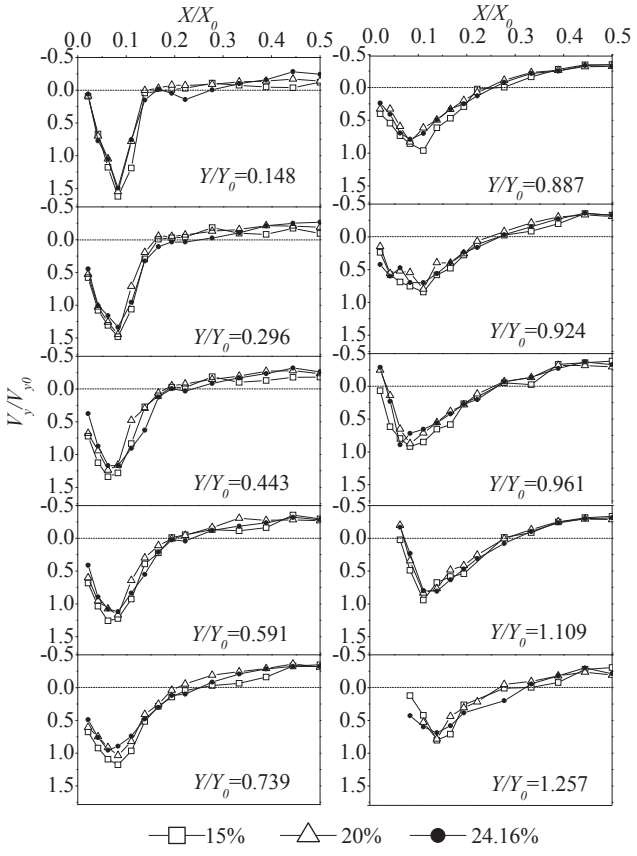

Fig. 6. Distribution curves of the dimensionless vertical velocity component for gas at different tertiary air ratios.

3. Results and discussion

The vertical velocity distribution curves of gas and particles phases are shown in Figs. 6 and 7. The distribution curves of the two phases are very similar. According to the coordinate direction in the Fig. 4, the vertical downward velocity is positive, and the result shows that the velocity near the furnace center (X/

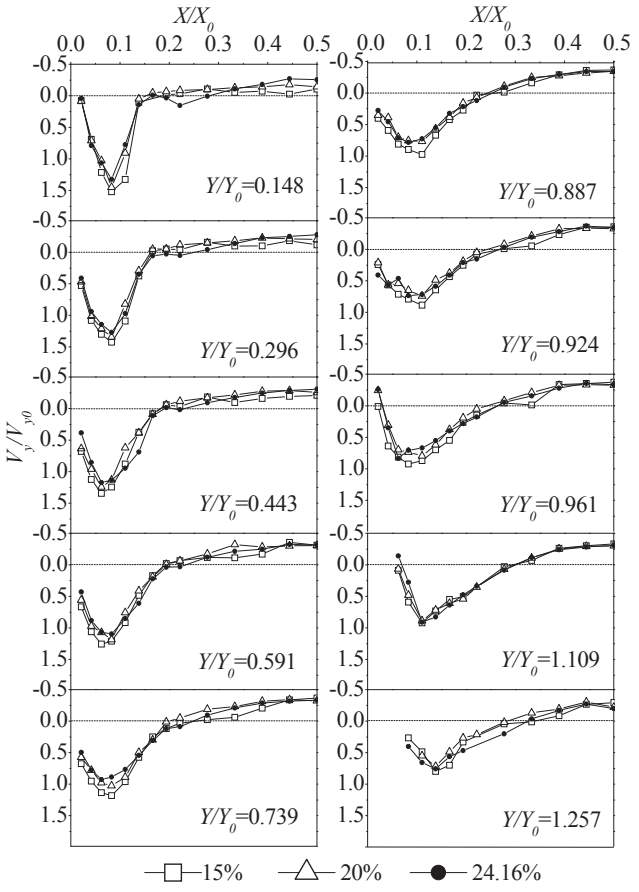

Fig. 7. Distribution curves of the dimensionless vertical velocity component for particles at different tertiary air ratios.

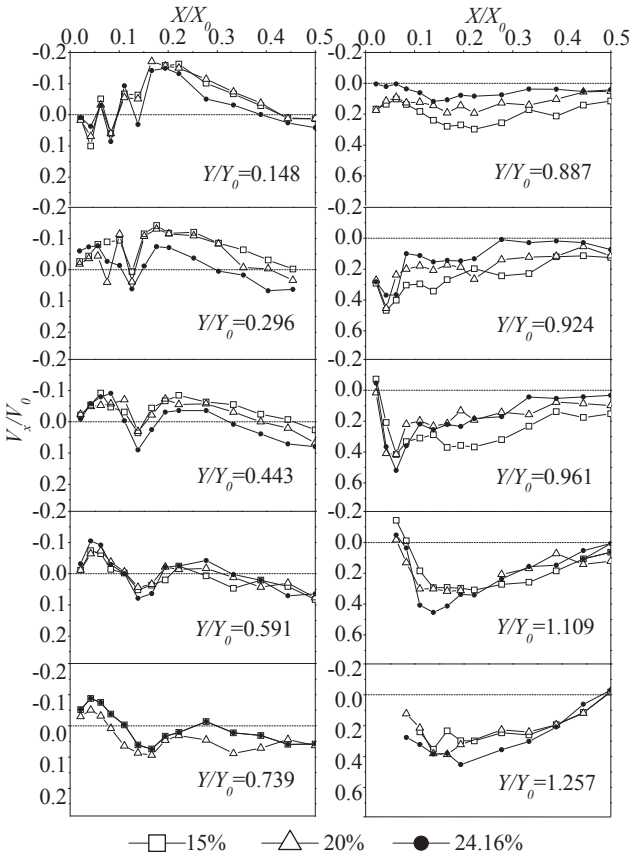

Fig. 9. Profiles of the dimensionless horizontal velocity distribution for gas at different tertiary air ratios.

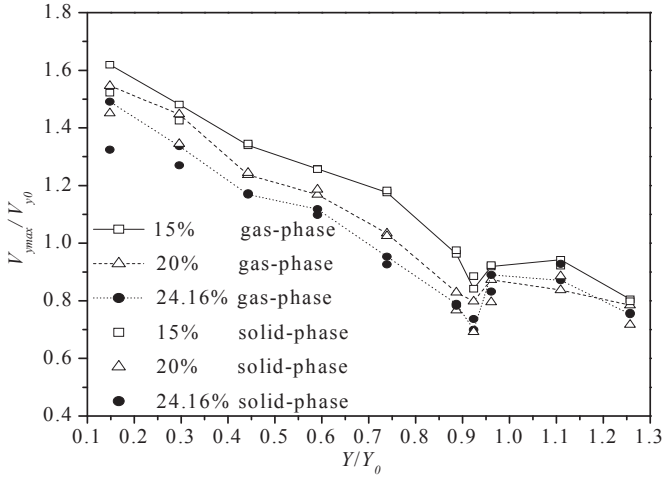

Fig. 8. Maximum velocity decay curves for gas and particle phase in the vertical direction.

$X_0 = 0.5$) is negative, while that near the side wall ($X/X_0 = 0$) is positive. This means that the gas–solid two-phase flow goes downward near the side wall and moves upward in the furnace center region and then a U shape flow field formed in the half furnace. We can speculate that the trajectory of the airflow in the whole furnace is W shape, consistent with that the expected design velocity at the furnace center is upward. The primary and secondary air near the side walls are injected downwards into the furnace. The inner and the outer secondary air are injected into the furnace at the same velocity, and the velocity is larger than that of the primary air. Due to the secondary air diffuse to the water wall, the velocity decays faster, so the outer secondary air velocity (near $X/X_0 = 0.04$) is slightly less than that of the inner secondary air velocity. Moreover, the vent air velocity which is entrained by the inner and outer secondary air has an intermediate value and therefore the gas phase velocity exhibits a peak near the location where the secondary air is injected ($X/X_0 = 0.08$). With the injection of the secondary air, the solid phase of primary and vent air gradually mixes with the secondary air and therefore the velocity increases. At the cross-section $Y/Y_0 = 0.148$, the maximum value of V_y/V_{y0} reaches 1.32–1.42, and the peak value of the velocity of the solid phase is slightly less than that of the gas phase. As the airflow is injected downwards it gradually decays and moves toward the furnace center. Because the total ratio of the over-the-arch air and the tertiary air are kept constant, when the tertiary air ratio increases, the over-the-arch secondary air ratio decreases, and the maximum velocity of the over-the-arch secondary air in each cross-sections declines. After the tertiary air section ($Y/Y_0 = 0.924$–1.257), as the tertiary air inject into the furnace with angle 25°, the airflow moves faster to the furnace center owing to the larger horizontal and vertical momentum. At the cross-section $Y/Y_0 = 1.109$–1.257, the differences in velocity are small.

Fig. 8 shows the maximum velocity decay curves for the gas and particle phases in the vertical direction. Before reaching the tertiary air nozzle ($Y/Y_0 = 0.148$–0.887), the maximum velocities of gas and

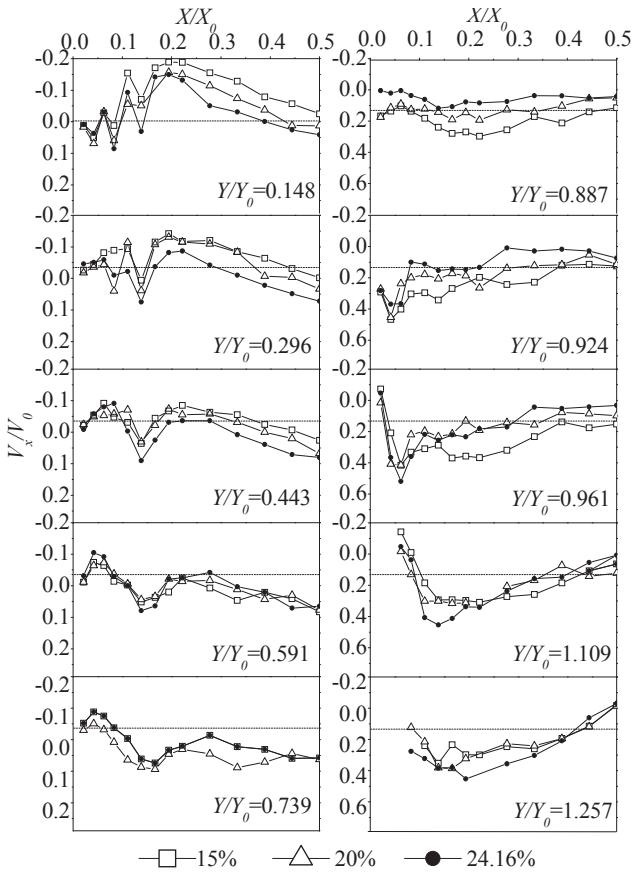

Fig. 10. Profiles of the dimensionless horizontal velocity distribution for particles at different tertiary air ratios.

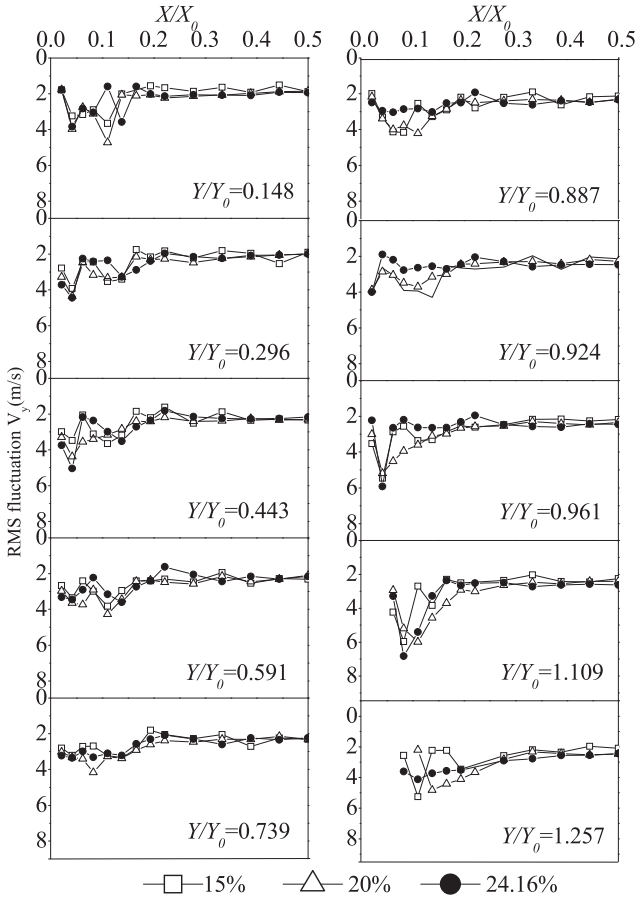

Fig. 11. Profiles of the vertical fluctuation rms velocity for the gas at different tertiary air ratios.

particles decrease. At the cross-section Y/Y_0 = 0.148–0.296, the maximum velocity of particles is lower than those of the gas phase, with the former being about 0.89–0.94 times of the latter. The reason for this is that the primary air velocity is lower than that of the secondary air, and after mixing with the secondary air, the velocity of the particles gradually increases because of the secondary air flow. At the cross-section Y/Y_0 = 0.443–1.257, the maximum velocities of both gas and particles are close. After arrival at the cross-section Y/Y_0 = 0.924–1.257, affect by the horizontal and vertical momentum of the tertiary air, the velocities of both the gas and particle phases increase slightly, and then gradually decline. The over-the-arch secondary air ratio decreases when the tertiary air ratio increases, the area keep constant so the initial velocity of over-the-arch air decreases. Therefore, before mixing with the tertiary air (at the cross-section Y/Y_0 = 0.148–0.887), the maximum vertical velocities at the same measurement points decrease as the tertiary air ratio increases, and after mixing with the tertiary air, the differences between the three cases are small.

Figs. 9 and 10 illustrate the horizontal velocity distribution for gas and particles, respectively. The movement trends of them are almost the same. The data distribution patterns are similar when the tertiary air rations change, as the nozzles on the arches inclines to the furnace center and 5° angle to the vertical direction. So that from the cross-section Y/Y_0 = 0.148 to Y/Y_0 = 0.887, the horizontal components of velocity are all small. The horizontal velocity is positive means the airflow and solid particles move to the furnace while negative means move to the front wall. There is negative horizontal velocity from the cross-section Y/Y_0 = 0.148 to 0.887, illustrating that there is recirculation zone beneath the burners, reflux entrainment high temperature gas, this is conducive to the ignition of the pulverized coal. At the cross-section Y/Y_0 = 0.148, which is nearest to the burner nozzles, the negative horizontal velocity is large. It means that the larger the flux velocity the more the entrainment heat; this is conducive to the ignition of the pulverized coal.

The under-the-arch reflux velocity decreases as the tertiary air ratio increases; because the secondary air volume decreases as the tertiary air ratio increases, the total volume near the cross-section decline and the avenue velocity reduces. At the cross-section Y/Y_0 = 0.887, before reaching the tertiary air nozzle the horizontal velocity for case is all positive, recirculation zone disappear, the airflow all moves to the furnace center. Beyond the cross-section Y/Y_0 = 0.924, the tertiary air injects into the furnace with a large momentum, horizontal velocity of the airflow near the front wall increases obviously and moves fast to the furnace center. As the airflow injects downward into the furnace, the peak of the horizontal velocity moves to the furnace center gradually. At the cross-section Y/Y_0 = 1.109 and Y/Y_0 = 1.257, the maximum value of the tertiary air horizontal velocity increases with an increase in the tertiary air ratio and the pulverized coal airflow moves more easily towards the furnace center.

The profiles of the vertical fluctuation velocities for the gas and solid phase are shown in Figs. 11 and 12. Both phases exhibit similar behavior. At each section, the primary and secondary air jet region has the larger fluctuation in velocity, while the fluctuation in velocity of the furnace center is smaller. This indicates that the airflow near the furnace center is stable, and with stable combustion in the

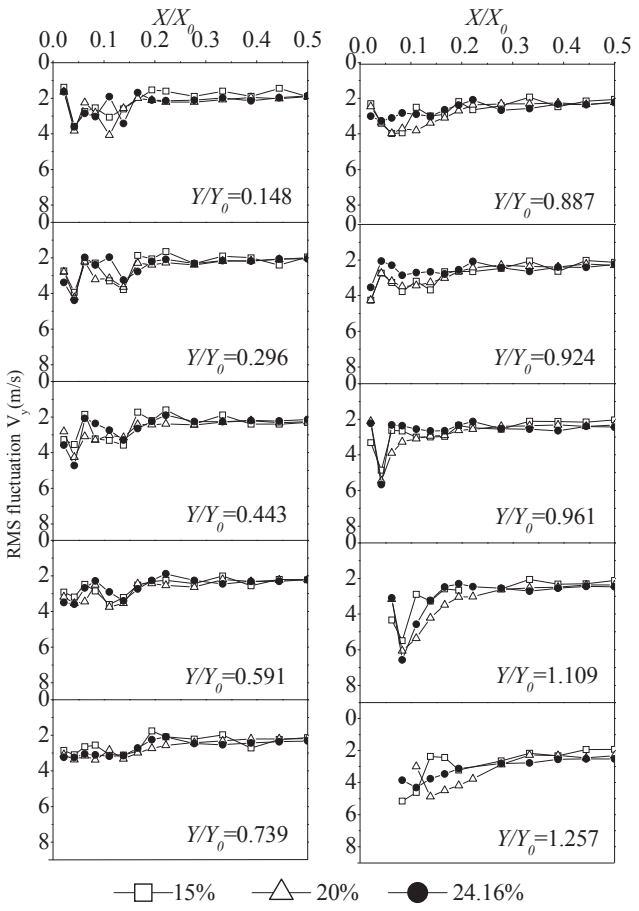

Fig. 12. Profiles of the vertical fluctuation rms velocity for the particles at different tertiary air ratios.

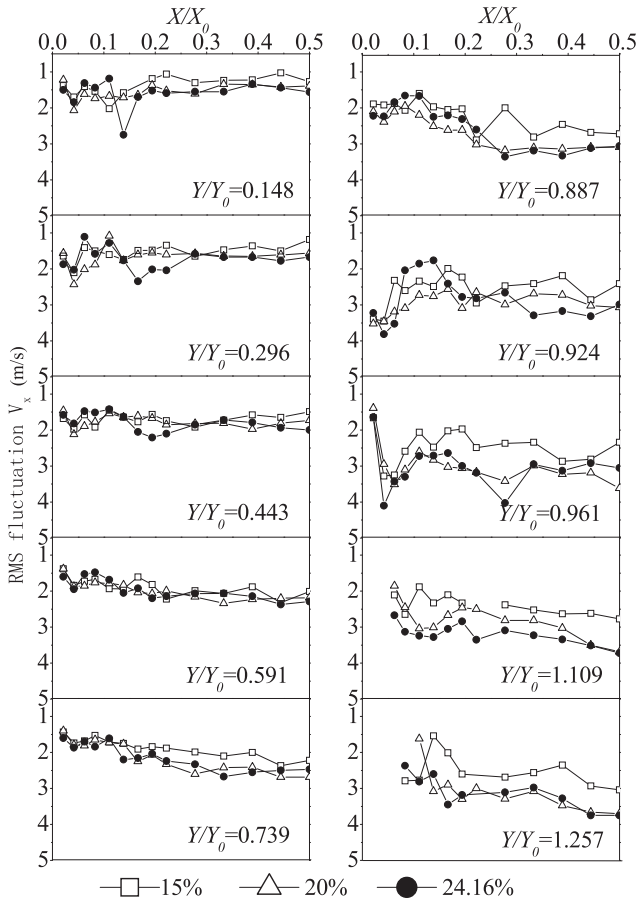

Fig. 13. Profiles of the horizontal fluctuation rms velocity for the gas at different tertiary air ratios.

boiler, the negative pressure fluctuation in the furnace will also be smaller. from the cross-section $Y/Y_0 = 0.961$ to 1.257, the vertical fluctuation velocity near the furnace hopper wall increases unexpectedly because of the on-the-arch airflow intersecting with the tertiary air at this point. The airflow undergoes intense mixing here. The gas phase represents the airflow in the furnace and the solid phase represents the pulverized coal flow in the furnace. So although the measurements are based on cold laboratory scale model we can infer that the high temperature pulverized coal ignition airflow mixes with the tertiary air intensely, and the O_2 that the pulverized coal combustion needed gets added and has fully combustion.

Figs. 13 and 14 depict the profiles of the horizontal fluctuation velocity distributions for gas and particles respectively. From the cross-section $Y/Y_0 = 0.148$ to $Y/Y_0 = 0.443$, the primary and secondary air gradually mix beneath the pulverized coal flow close to the front/rear wall and the secondary air. With the injection of the secondary air, the primary air moves horizontally; therefore, the horizontal fluctuation velocity is larger while the fluctuation velocity of the furnace center is smaller. The disturbance is also smaller. For the horizontal fluctuation velocity, the gas velocity is larger than that of the solid. The injection function effect on gas phase flow is much more clearly seen, while the solid particles exhibit a smaller disturbance owing to their large inertia. Between the cross-section $Y/Y_0 = 0.443$ and $Y/Y_0 = 0.739$, the fluctuation velocity is small because the mix of the primary air and the secondary air is uniform. At the cross-section $Y/Y_0 = 0.924$–1.257, the airflow intersects owing to the supply of tertiary air. The horizontal fluctuation velocities of both the gas phase and solid phase increase, and the disturbances of the two phases are intense in the area near the front/rear wall and the furnace center. In terms of combustion, a larger fluctuation velocity is conducive to improved mixing of the pulverized coal ignition airflow and the tertiary air, mass transfer and heat transfer enhancement favors the full combustion of the pulverized coal.

Fig. 15 depicts the distribution of the mean diameter of the particles. The mean value is obtained by considering particles having a diameter in the range 0–100 μm. Along the six cross-sections from $Y/Y_0 = 0.148$ to $Y/Y_0 = 0.887$, there are no discernable differences between the distribution at the furnace center and that of the region next to the front/rear wall. However, below the tertiary air stream, especially after entering the hopper area, the particle diameters at the area next to the water-cooled wall begin to increase and are remarkably obvious at the cross-section $Y/Y_0 = 1.109$. The larger the amount of over-the-arch air, the larger is the penetrating depth of the air flow. As the ratio of the tertiary air decreases, its ability to intercept the airflow declines, so that the particles with relatively large diameters separate out. This, in turn, can easily lead to the abrading and slagging of the furnace hopper while larger ratios of the tertiary air can reduce such tendencies.

The distribution of the particle volume flux is shown in Fig. 16. It can be seen that there is only one peak for the volume flux from the cross-section $Y/Y_0 = 0.148$ to $Y/Y_0 = 0.961$. The peak corresponds to a location below the fuel-rich nozzles. In contrast, fuel-lean flow occurs between the inner secondary air and outer secondary air, mixing with

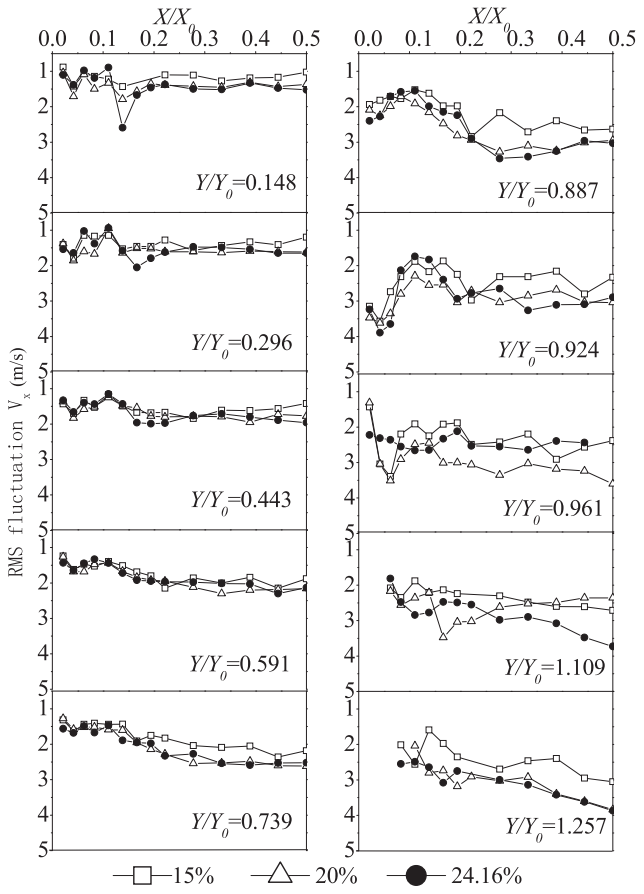

Fig. 14. Profiles of the horizontal fluctuation rms velocity for the particles at different tertiary air ratios.

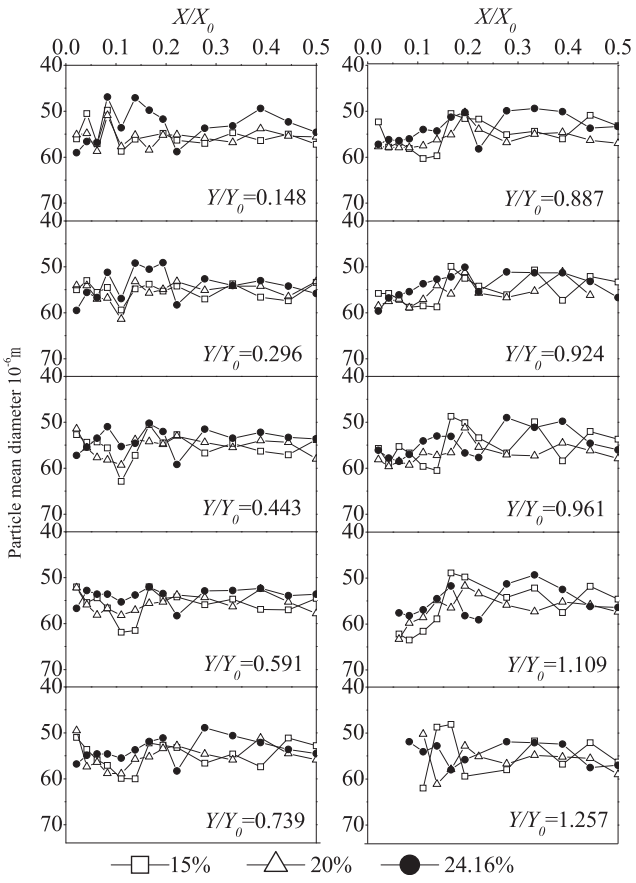

Fig. 15. Distribution of the particle diameters at different tertiary air ratios.

them just after flowing from the nozzles so that there are no peaks. As the flow goes downwards, the fuel-rich stream gradually mixes with the secondary air, vent air and the exiting secondary air. This is reflected in the continuing decline of the peak value and the gradual increase of the width of the peak region. Such behavior indicates that the pulverized coal particles diffuse towards the furnace center and the inner secondary air direction. The gradual decline of the peak value also illustrates that short-circuiting of the fuel-rich flow does not occur. In fact, this assists the staged combustion of the pulverized coal and the stability of the flame when pulverized coal particles penetrate to the secondary air in a gradual manner.

Fig. 17 shows the decay curves of the maximum particle volume flux as a function of the height. Above the cross-section $Y/Y_0 = 0.591$, the maximum particle volume flux exhibits a relatively large decay, showing that the solid-phase particles quickly mix with the over-the-arch air. The maximum particle volume fluxes along the cross-section $Y/Y_0 = 0.148$, under different tertiary air ratios of 15%, 20% and 24.16%, are 3.9×10^{-4}, 4.6×10^{-4} and 6.6×10^{-4} m^3 m^{-2} s, respectively. With an increase in the tertiary air ratio, the amount of the over-the-arch secondary air decreases so that the injecting behavior of the secondary air on the primary air decreases. Meanwhile, the maximum particle volume flux at the same measurement point increases, leading to an increase of the pulverized coal concentrate, and a decrease of the ignition heat, a feature that is beneficial to ignition of the pulverized coal. Beyond the cross-section $Y/Y_0 = 0.591$, the decay of the maximum particle volume flux become flat, and the mixing between the particle phase and gas phase becomes uniform so that there are essentially no differences between the various cases.

The maximum gas-phase vertical velocity and the distribution of the locations for the maximum solid-phase particles volume flux are shown in Fig. 18. The maximum gas-phase vertical velocity of the airflow ahead of the tertiary air nozzles is the velocity of the over-the-arch secondary air. After mixing with the tertiary air; the maximum gas-phase vertical velocity becomes the maximum gas-phase vertical velocity of the mixture. The location of the maximum solid-phase volume flux stands for the trajectory of the fuel-rich flow. For both the over-the-arch secondary air and the primary air traveling downwards beneath the arch and next to the front wall, the locations of the maximum gas phase vertical velocity are next to the front wall. The trajectory of the fuel-rich flow is near the furnace center. Compare with Refs. [6–9], the over-the-arch secondary air and the primary air mixed slowly which benefit to prolong the remaining time at low oxygen atmosphere. The whole flow tends towards the front wall before reaching the tertiary air. After reaching the tertiary air, the flow continues in a downward direction, next to the furnace hopper, and there is intensive mixing between the particle phase and the gas phase. As the tertiary air ratio increases, the locations of the maximum gas-phase vertical velocity and the maximum solid-phase particle volume flux are positioned further away from the furnace hopper. The particle phase could reach the center of furnace hopper which means the long remaining time of the pulverized coal. Multi-injection and multi-stage combustion technology absorbing of a 25° declination angle (From Ref. [23]) of territory air was the successful design. This feature

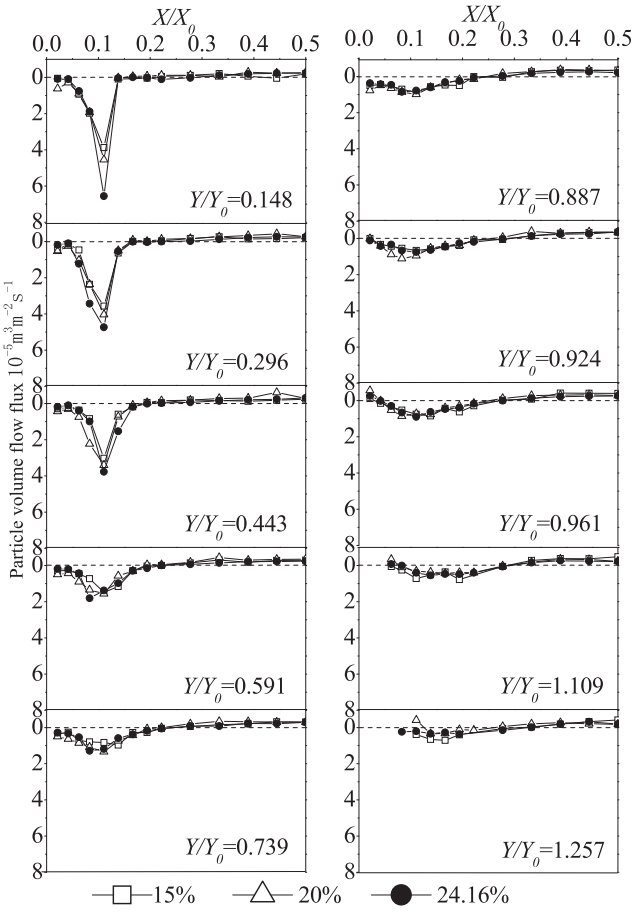

Fig. 16. Distribution of the particle volume flux at different tertiary air ratios.

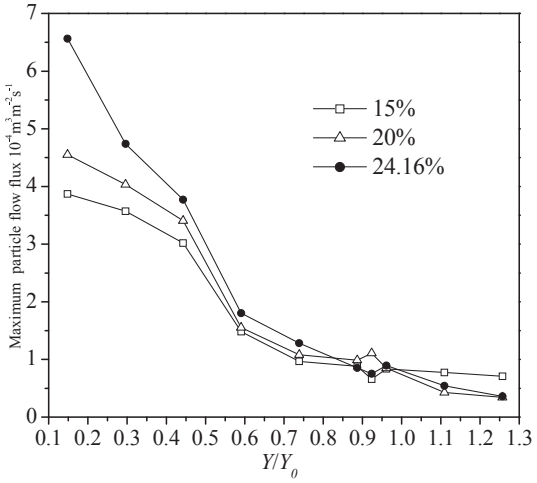

Fig. 17. Decay curves of the maximum particle volume flux at different tertiary air ratios.

decreases the possibility of flushing the hopper and also makes slagging in the hopper less likely.

4. Conclusion

PDA system was used to study the gas–solid two-phase flow characteristics of a down-fired 350 MWe supercritical utility boiler, a 1:20 model was built for the research, the results showed that:

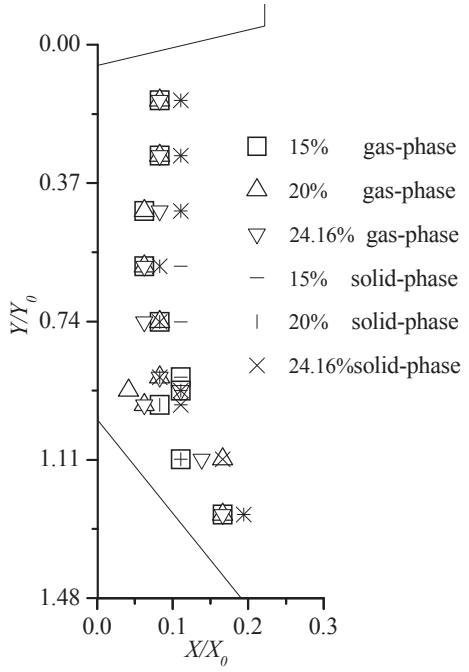

Fig. 18. Distribution of the location of the vertical maximum air velocity and the maximum particle volume flux at different tertiary air ratios.

1) The gas and solid particles move downward near the side wall, and move upward in the furnace center area, and then a U shape flow field formed in the half furnace.
2) There is negative horizontal velocity from the cross-section $Y/Y_0 = 0.148$ to 0.887. At the cross-section $Y/Y_0 = 0.148$, which is nearest to the burner nozzles, the negative horizontal velocity is the largest, illustrating that there is recirculation zone beneath the burners.
3) From the cross-section $Y/Y_0 = 0.961$ to $Y/Y_0 = 1.257$, the horizontal/vertical fluctuation velocity for gas/solid phases near the furnace hopper wall increases unexpectedly, the airflow intense mixing here.
4) Here is one peak for the particle volume flux below the primary air nozzle and the peak value drops as the flow travels downwards. From the cross-section $Y/Y_0 = 0.148$ to $Y/Y_0 = 0.591$, the decay velocity of the maximum particle volume flux was relatively sharp. At the cross-section $Y/Y_0 = 0.148$, the maximum volume flux increased obviously, and is conducive for the pulverized coal to ignite. Beyond the cross-section $Y/Y_0 = 0.591$, the gas phase and the solid phase then mixed uniform gradually.
5) The particle diameter increased obviously close to the furnace hopper beneath the tertiary air nozzle and the particle diameter decreased with the increase of tertiary air; the locations of the gas-phase vertical maximum velocity and the solid-phase particles maximum volume flux moved further away from the hopper. This feature reduced the possibility of the occurrence of both flushing and slagging of the hopper.

Acknowledgments

This work was supported by the Foundation for Innovative Research Groups of the National Natural Science Foundation of China (Grant No. 51121004).

References

[1] Fan WD, Lin ZC, Li YY, Kuang JG, Zhang MC. Effect of air-staging on anthracite combustion and NOx formation. Energy & Fuels 2009;23:111–20.
[2] Tan HZ, Niu YQ, Wang XB, Xu TM, Hui SE. Study of optimal pulverized coal concentration in a four-wall tangentially fired furnace. Appl Energy 2011;88:1164–8.
[3] Plumed A, Cañadas L, Otero P, Espada MI, Gonzálcz JF. Primary measures for reduction of NOx in low volatile coals combustion. Coal Sci Technol 1995;24:1783–6.
[4] Xu XC, Wang YS, Jin ML, Zhao P. The function of the pulverized coal pulverized coal flame stability, the precombustion chamber and the flame stabilization ship. J Eng Therm Phys 1988;9:384–9 [in Chinese].
[5] Jiang PZ, Shi XG, Xu XC. Experimental study on three-dimensional turbulent flow field of the pulverized coal flat burner which has the flame stabilization ship. J Eng Therm Phys 1990;11:109–11 [in Chinese].
[6] Wang HJ, Huang ZF, Wang DD, Luo ZX, Sun YP. Measurements on flame temperature and its 3D distribution in a 660 MWe arch-fired coal combustion furnace by visible image processing and verification by using an infrared pyrometer. Meas Sci Technol 2009;20:4006–17.
[7] Ren F, Li ZQ, Liu GK, Chen ZC, Zhu QY. Combustion and NOx emissions characteristics of a down-fired 660-MWe utility boiler retro-fitted with air-surrounding-fuel concept. Energy 2011;36:70–7.
[8] Fan SB, Li ZQ, Yang XH, Liu GK, Chen ZC. Influence of outer secondary-air vane angle on combustion characteristics and NOx emissions of a down-fired pulverized-coal 300 MWe utility boiler. Fuel 2010;89:1525–33.
[9] Li ZQ, Kuang M, Zhang J, Han YF, Zhu QY, Yang LJ. Influence of staged-air on airflow, combustion characteristics and NOx emissions of a down-fired pulverized-coal 300 MWe utility boiler with direct flow split burners. Environ Sci Technol 2010;44:1130–6.
[10] Burdett NA. The effects of air staging on NOx emissions from a 500 MW(e) down-fired boiler. J Inst Energy 1987;60:103–7.
[11] Kuang M, Li ZQ, Xu ST, Zhu QY. Improving combustion characteristics and NOx emissions of a down-fired 350 MWe utility boiler with multiple injection and multiple staging. Environ Sci Technol 2011;45:3803–11.
[12] Kuang M, Li ZQ, Zhang Y. Asymmetric combustion characteristics and NOx emissions of a down-fired 300 MWe utility boiler at different boiler loads. Energy 2011;37:580–90.
[13] Miao CX, Wang JW. Analysis of “asymmetric burning” problem in a W-shaped flame boiler of 600 MW unit. Therm Power Gener 2005;34:48–51 [in Chinese].
[14] Fang QY, Wang HJ, Wei Y, Lei L, Duan XL, Zhou HC. Numerical simulations of the slagging characteristics in a down-fired, pulverized-coal boiler furnace. Fuel Process Technol 2010;91:88–96.
[15] Fan JR, Liang XH, Xu QS, Zhang XY, Cen KF. Numerical simulation of the flow and combustion processes in a three-dimensional, W-shaped boiler furnace. Energy 1997;22:847–57.
[16] Cañadas L, Cortés V, Rodríguez F, Otero P, González JF. NOx reduction in arch fired boilers by parametric turning of operating conditions. In: Proceedings of the electric power research institute (EPRI)/environmental protection agency (EPA) megasymposium Washington, D.C., USA; 1997.
[17] Fueyo N, Gambón V, Dopazo C, González JF. Computational evaluation of low NOx operating conditions in arch-fired boilers. J Eng Gas Turbines Power 1999;121:735–40.
[18] Leisse A, Lasthaus D. New experience gained from operating DS (swirl stage) burners, vol. 88. VGB Power Tech; 2008. p. 43–9.
[19] Garcia-Mallol JA, Steitz T, Chu CY, Jiang PZ. Ultra-low NOx advanced FW arch firing: central power station applications. In: Proceedings of the 2nd U.S. China NOx and SO_2 control workshop, Dalian, China; 2005.
[20] Zhou ZJ, Zhu ZL, Zhao X, Yao Q, Cao XY, Cen KF. The effect of swirling number on the flow field of down shot flame furnace. Power Eng 1999;19:33–7 [in Chinese].
[21] Fan WD, Li YY, Lin ZC, Zhang MC. PDA research on a novel pulverized coal combustion technology for a large utility boiler. Energy 2010;35:2141–8.
[22] Ren F, Li ZQ, Chen ZC, Xu ZX, Yang GH. Experimental investigations into gas/particle flows in a down-fired boiler: influence of the vent air ratio. Energy Fuels 2010;24:1592–602.
[23] Li ZQ, Ren F, Chen ZC, Liu GK, Xu ZX. Experimental investigations into gas/particle flows in a down-fired boiler: influence of down-draft secondary air. Energy & Fuels 2009;23:5846–54.
[24] Kuang M, Li ZQ, Zhu QY. Gas/particle flow characteristics, combustion and NOx emissions of down-fired 600 MWe supercritical utility boilers with respect to two configurations of combustion systems. Energy & Fuels 2012;26:3316–28.
[25] Kuang M, Li ZQ, Zhu QY, Wang Y, Chen LZ, Zhang Y. Experimental gas/particle flow characteristics of a down-fired 600 MWe supercritical utility boiler at different staged-air ratios. Energy 2012;42:411–23.
[26] Kuang M, Li ZQ, Zhu QY, Zhang Y. Performance assessment of staged-air declination in improving asymmetric gas/particle flow characteristics within a down-fired 600 MWe supercritical utility boiler. Energy 2013;49:423–33.
[27] Liu CL, Li ZQ, Jing XJ, Xie YQ, Zhang QH, Zong QD. Experimental investigation into gas/particle flow in a down-fired 350 MWe supercritical utility boiler at different over-fire air ratios. Energy 2014;64:771–8.
[28] Kuang M, Li ZQ, Zhu QY, Zhang HY. Characterization of gas/particle flows with respect to staged-air ratio for a down-fired 600 MWe supercritical utility boiler with multiple injection and multiple staging: a lab-scale study. Int J Therm Sci 2013;70:154–65.
[29] Liu CL, Li ZQ, Zhang X, Jing XJ, Zhang WZ, Chen ZC, et al. Aerodynamic characteristics within a cold small-scale model for a down-fired 350 MWe supercritical utility boiler at various primary air to vent air ratios. Energy 2012;47:294–301.
[30] Lin ZC, Fan WD, Li YY, Li YH, Zhang MC. Research of low NOx combustion with large-angle counter flow of a fuel-rich jet and its particle-dynamics anemometer (PDA) experiment. Energy & Fuels 2009;23:744–53.
[31] Mathiesen V, Solberg T, Hjertager BH. An experimental and computational study of multiphase flow behavior in a circulating fluidized bed. Int J Multiph Flow 2000;26:387–419.
[32] Gillandt I, Fritsching U, Bauckhage K. Measurement of phase interaction in dispersed gas/particle two-phase flow. Int J Multiph Flow 2001;27:1313–32.

Nomenclature

OFA: over-fire air
X_0: horizontal distance in the lower furnace between the front and rear walls
X: distance from the coordinate origin to the measurement point in the horizontal direction
Y_0: vertical distance between the fuel-rich flow nozzle outlet and the hopper upper edge
Y: vertical distance from the measurement point to the fuel-rich flow nozzle outlet
V_y: vertical velocity of the measurement point (m/s)
V_{y0}: vertical velocity of the primary air outlet (m/s)